Khakalo, Sergei; Balobanov, Viacheslav; Niiranen, Jarkko

Modelling size-dependent bending, buckling and vibrations of 2D triangular lattices by strain gradient elasticity models: applications to sandwich beams and auxetics

Published in:
International Journal of Engineering Science

DOI:
10.1016/j.ijengsci.2018.02.004

Published: 01/06/2018

Document Version
Peer-reviewed accepted author manuscript, also known as Final accepted manuscript or Post-print

Please cite the original version:
Khakalo, S., Balobanov, V., & Niiranen, J. (2018). Modelling size-dependent bending, buckling and vibrations of 2D triangular lattices by strain gradient elasticity models: applications to sandwich beams and auxetics. *International Journal of Engineering Science*, *127*, 33-52. https://doi.org/10.1016/j.ijengsci.2018.02.004

Modelling size-dependent bending, buckling and vibrations of 2D triangular lattices by strain gradient elasticity models: Applications to sandwich beams and auxetics

Article *in* International Journal of Engineering Science · June 2018
DOI: 10.1016/j.ijengsci.2018.02.004

3 authors:

Sergei Khakalo
Aalto University

Viacheslav Balobanov
Aalto University

Jarkko Niiranen
Aalto University

Modelling size-dependent bending, buckling and vibrations of 2D triangular lattices by strain gradient elasticity models: applications to sandwich beams and auxetics

Sergei Khakalo*, Viacheslav Balobanov* and Jarkko Niiranen*

*Aalto University, School of Engineering, Department of Civil Engineering, P.O. Box 12100, 00076 AALTO, Finland.

February 23, 2018

Abstract

The present work is devoted to the modelling of strongly size-dependent bending, buckling and vibration phenomena of 2D triangular lattices with the aid of a simplified first strain gradient elasticity continuum theory. As a start, the corresponding generalized Bernoulli–Euler and Timoshenko sandwich beam models are derived. The effective elastic moduli corresponding to the classical theory of elasticity are defined by means of a computational homogenization technique. The two additional length scale parameters involved in the models, in turn, are validated by matching the lattice response in benchmark problems for static bending and free vibrations calibrating the strain energy and inertia gradient parameters, respectively. It is demonstrated as well that the higher-order material parameters do not depend on the problem type, boundary conditions or the specific beam formulation. From the application point of view, it is first shown that the bending rigidity, critical buckling load and eigenfrequencies strongly depend on the lattice microstructure and these dependencies are captured by the generalized Bernoulli–Euler beam model. The relevance of the Timoshenko beam model is then addressed in the context of thick beams and sandwich beams. Applications to auxetic strut lattices demonstrate a significant increase in the stiffness of the metamaterial combined with a clear decrease in mass. Furthermore, with the introduced generalized beam finite elements, essential savings in the computational costs in computational structural analysis can be achieved. For engineering applications of architectured materials or structures with a microstructure utilizing triangular lattices, generalized mechanical properties are finally provided in a form of a design table for a wide range of mass densities.

Keywords: Strain gradient elasticity, Lattice structures, Bernoulli–Euler beam, Timoshenko beam, Size dependency, Bending rigidity, Critical buckling load, Eigenfrequencies, Architectured materials, Sandwich structures, Auxetics, Reentrant honeycombs, Mechanical metamaterials

1 Introduction

Beams as structural elements have been widely used in scientific and industrial applications of various fields. Nowadays, with fast developing manufacturing technologies, the application domain constantly expands from covering the classical civil and mechanical engineering applications towards, e.g., micro- and nanoelectromechanical systems (MEMS/NEMS), lattice structures at both macro- and, especially, micro/nano-scales. One of the most crucial issues from the point of view of engineering sciences is the prediction of the mechanical behaviour of such structures in an accurate and versatile way. Accordingly, material modeling in its broad meaning plays a pivotal role for achieving this goal.

Cauchy continuum mechanics can be efficiently used for predicting the mechanical response of a wide range of natural and (artificial) metamaterials. However, the increasing complexity of materials, or structures (with highly noticeable, architectured microstructure), across the scales requires advanced modeling techniques. Generalized continuum theories have been shown to be able to account for the microstructures at the continuum level and, hence, to provide much more reliable prediction of material behaviour (see the reviews and discussion in [1, 2, 3]). Even more, the fundamental principles underlying the theories of generalized continua do not limit the characteristic sizes of microstructures. As clarified in [4], term "micro" refers to the characteristic scale of a substructure and hence reflects the scales lower than those of the real object (without any limitations to the micrometer scale).

Two branches of generalized continuum theories can be distinguished: "higher-order" theories in which the number of degrees of freedom increases [5, 6, 7, 8, 9], and "higher-grade/gradient" theories in which the higher gradients of displacements (or strains) are included [10, 6, 11, 12]. The first strain (second displacement) gradient and couple-stress theories (especially their modified versions [13, 14]) are perhaps the simplest and, hence, the most utilized non-standard continuum models. In the present work, we restrict ourselves to the strain gradient continuum theories. In detail, we develop and apply gradient-elastic variants of Bernoulli–Euler and Timoshenko beam models and show that they accurately and efficiently model structural beams having a lattice microstructure. In literature, generalized beam model formulations within different (1) beam theories, e.g., Bernoulli–Euler, Timoshenko and higher-order shear-deformable beam models, (2) beam structure types, e.g., sandwich and functionally graded beams, (3) non-classical continuum theory type, e.g., strain gradient and couple-stress theories, have been actively developed during the past years [15, 16, 17, 18, 19, 20, 21, 22, 23, 24]. However, most of these contributions focus on model derivations and analytical solutions for academic benchmark problems without enlarging the domain of practical applications, including numerical methods enabling the analysis of complex systems beyond the simplest benchmarks. Some exceptions can be found in [25, 26, 27], and this contribution is aimed to serve as another point of view in this direction.

Higher-order material moduli of generalized continuum theories (typically considered to be micro-structural length scale parameters) have been considered as an inconvenient addition implied by the generalizations. Quite recently, however, there has been many attempts to address the role of these material parameters and to quantify them. For instance, [15, 28, 29] consider static bending tests at micrometer- and nanometer-scales, whereas the micro-inertia length scale parameter has been assessed in [30] by experiments on torsional vibrations fo fine-grained materials, and atomistic representations of elastic moduli tensors for different materials have been provided in [31]. Altogether, literature on applications of non-classical continuum models to real materials, structures and systems is still very limited; some examples can be found in [32, 33, 34, 35, 36, 37, 38, 39]. Regarding numerical methods and numerical analysis for the models of generalized continuum mechanics, literature is limited as well, although there are some successful endeavours including rigorous studies on solvability and convergence (for recent overviews and examples, see [40, 41, 25, 42, 26, 43, 44, 45]).

In the present work, we address four fundamental issues arising around non-classical continuum theories in the context of structural models and applications: (1) selection of an appropriate generalized theory type, (2) identification of the higher-order material parameters/moduli, (3) application to real materials and structures independent of the length scale, (4) general-purpose numerical methods versatile for problems with complex geometries. The main novelties and findings of the present work are detailed as follows:

(i) We derive strain gradient Bernoulli–Euler and Timoshenko models for sandwich beams – by following the so-called engineering sandwich beam theory – involving one micro-structural and one micro-inertia length scale parameter.

(ii) We demonstrate the size-dependent mechanical response of 2D triangular lattice structures in bending and calibrate both the micro-structural and micro-inertia length scale parameters by utilizing the strain gradient Bernoulli–Euler beam model.

(iii) We approve that the length scale parameters are material moduli in the sense that they are independent of the problem type (statics or dynamics), boundary condition types (including both kinematic and static boundary conditions) and beam models (Bernoulli–Euler or Timoshenko models for conventional or sandwich structures).

(iv) For auxetic metamaterials, exhibiting bending dominated deformations of the struts forming the material architecture, we (1) propose a micro-architectured modification which leads to an essential increase in structural stiffness with an essential decrease in mass, and (2) build a gradient-elastic beam model and perform numerical simulations by proposing a modification for standard beam elements of a commercial finite element software.

This article is organized as follows: In Section 2, we at first briefly recall the fundamentals of the first strain (second displacement) gradient elasticity theory for isotropic materials and then derive the elasto-dynamic equations of the corresponding generalized Bernoulli–Euler and Timoshenko beam models corresponding to the so-called engineering sandwich beam theory. Section 3 is devoted to computational homogenization procedure applied to triangular lattices. In Section 4, we first analyse the size-dependent mechanical response of a 2D triangular lattice by considering three problem settings: static bending, static buckling and free vibrations. The generalized Bernoulli–Euler beam model is then utilized for calibrating the two length scale parameters involved. In Section 5, we demonstrate the relevance of the generalized Timoshenko beam model for both static and dynamic regimes. Section 6 is devoted to applications of strain gradient beams to auxetics. Finally, Section 7 contains discussions and conclusions.

2 Strain gradient elasticity for sandwich beams

In this section, the strain gradient elasticity theory is applied to sandwich beams. At first, we recall the variational formulation of the strain gradient elasticity theory with first velocity gradient inertia. Then, by utilizing the basic kinematical and stress assumptions for Bernoulli–Euler and Timoshenko beam models, we derive the corresponding generalized strong forms of the beam bending problems, i.e., the governing differential equations of elasto-dynamics with a set of boundary conditions. The derived strong formulations are generalized to multi-layer beams.

2.1 Variational formulation of strain gradient elasticity

Hamilton's principle for an independent displacement variation $\delta\boldsymbol{u}$ between fixed limits of displacement $\boldsymbol{u}$ of body $\Omega \subset \mathbb{R}^3$ at times t_0 and t_1 reads as [46]

$$\delta \int_{t_0}^{t_1} \int_{\Omega} (T - W) d\Omega dt + \int_{t_0}^{t_1} \delta W_1 dt = 0, \tag{2.1}$$

where δW_1 stands for the variation of the work done by external forces. Strain and kinetic energy densities W and T, respectively, are considered in the form [6]

$$W = \frac{1}{2} C_{ijkl} \varepsilon_{ij} \varepsilon_{kl} + \frac{1}{2} A_{mijnkl} \partial_m \varepsilon_{ij} \partial_n \varepsilon_{kl}, \tag{2.2}$$

$$T = \frac{1}{2} \rho \dot{u}_i \dot{u}_i + \frac{1}{2} \rho d_{ij} \partial_i \dot{u}_k \partial_j \dot{u}_k, \tag{2.3}$$

where C_{ijkl} and A_{mijnkl} stand, respectively, for components of the classical and higher-order stiffness tensors and d_{ij} are associated to the inertial length scale parameters.

It is assumed that the material is centrosymmetric with linearly elastic behaviour. Small deformation assumptions are adopted leading to the kinematical relation expressed in the form of engineering strains

$$\varepsilon_{ij} = \frac{1}{2}(\partial_i u_j + \partial_j u_i). \tag{2.4}$$

The variation of the total kinetic energy (for guidance, see [46], for instance) is derived in the form

$$\delta \int_{t_0}^{t_1} \int_{\Omega} T d\Omega dt = -\int_{t_0}^{t_1} \int_{\Omega} (\dot{p}_i \delta u_i + \dot{q}_{ij} \delta \partial_i u_j) d\Omega dt, \tag{2.5}$$

where $\boldsymbol{p}$, standing for the ordinary momentum vector, and $\boldsymbol{q}$, denoting the higher-order momentum tensor, are defined as the derivatives of the kinetic energy density with respect to the corresponding work conjugates, i.e., $\dot{\boldsymbol{u}}$ and $\nabla \dot{\boldsymbol{u}}$, as

$$p_i = \frac{\partial T}{\partial \dot{u}_i} = \rho \dot{u}_i, \quad q_{ij} = \frac{\partial T}{\partial(\partial_i \dot{u}_j)} = \rho d_{ik} \partial_k \dot{u}_j. \tag{2.6}$$

The variation of the total strain energy takes the form

$$\delta \int_{t_0}^{t_1} \int_{\Omega} W d\Omega dt = \int_{t_0}^{t_1} \int_{\Omega} (\tau_{ij}\delta\varepsilon_{ij} + \mu_{ijk}\delta\partial_i\varepsilon_{jk}) d\Omega dt, \tag{2.7}$$

where the Cauchy (or Cauchy-like) stress tensor $\boldsymbol{\tau}$, the work conjugate of the ordinary strain tensor $\boldsymbol{\varepsilon}$, and the double stress tensor $\boldsymbol{\mu}$, the work conjugate of the strain gradient tensor $\nabla\boldsymbol{\varepsilon}$, respectively, are defined as

$$\tau_{ij} = \frac{\partial W}{\partial \varepsilon_{ij}} = C_{ijkl}\varepsilon_{kl}, \quad \mu_{ijk} = \frac{\partial W}{\partial(\partial_i \varepsilon_{jk})} = A_{ijklmn}\partial_l \varepsilon_{mn}. \tag{2.8}$$

For isotropic materials, the conventional fourth-rank tensor of elastic constants becomes

$$C_{ijkl} = \mu(\delta_{ik}\delta_{jl} + \delta_{il}\delta_{jk}) + \lambda\delta_{ij}\delta_{kl}, \tag{2.9}$$

where μ and λ denote the Lamé parameters and δ_{ij} is a Kronecker symbol. In case of weak non-locality for isotropic materials [47], the sixth-rank constitutive tensor degenerates into

$$A_{mijnkl} = g^2 \delta_{mn} C_{ijkl}, \tag{2.10}$$

leading to the so-called simplified strain gradient elasticity model [13, 48] with g denoting an intrinsic structural length scale parameter with unit of length. For the second-rank micro inertia tensor, we adopt the following simplification:

$$d_{ij} = \gamma^2 \delta_{ij}, \tag{2.11}$$

where γ stands for an intrinsic inertial length scale parameter with unit of length.

For constant μ, λ and ρ, constitutive relations (2.6) and (2.8) take the simplified forms

$$\tau_{ij} = 2\mu\varepsilon_{ij} + \lambda\varepsilon_{kk}\delta_{ij}, \quad \mu_{ijk} = g^2 \partial_i \tau_{jk}, \quad p_i = \rho \dot{u}_i, \quad q_{ij} = \gamma^2 \partial_i p_j. \tag{2.12}$$

2.2 Generalized Bernoulli–Euler model for sandwich beams

Let us consider a long prismatic body and recall the derivation of Bernoulli–Euler beam bending model in the framework of the strain gradient elasticity theory (cf. [25]). For plane bending, the kinematic assumptions read as

$$u_x = -y w'(x,t), \quad u_y = w(x,t), \quad u_z = 0. \tag{2.13}$$

By following the basic assumptions regarding the beam model [49], constitutive relations (2.12) take the reduced form (see the details in Appendix A)

$$\tau_{xx} = E\varepsilon_{xx}, \quad \mu_{xxx} = g^2 E \partial_x \varepsilon_{xx}, \quad \mu_{yxx} = g^2 E \partial_y \varepsilon_{xx}, \tag{2.14}$$

where E denotes Young's modulus. For the five-parameter isotropic strain gradient model, the higher-order beam assumptions are highlighted in Appendix A.

By substituting assumptions (2.13) into (2.5) with (2.12), and into (2.7) with (2.4) and (2.14), one can derive the variations of the kinetic and strain energies, respectively, in the form

$$\delta \int_{t_0}^{t_1} \int_{\Omega} T d\Omega dt = - \int_{t_0}^{t_1} \int_0^L \int_A \rho(\ddot{w}\delta w + (y^2 + 2\gamma^2)\ddot{w}'\delta w' + y^2\gamma^2 \ddot{w}''\delta w'') dV dt, \tag{2.15}$$

$$\delta \int_{t_0}^{t_1} \int_{\Omega} W d\Omega dt = \int_{t_0}^{t_1} \int_0^L \int_A E((y^2 + g^2) w''\delta w'' + y^2 g^2 w'''\delta w''') dV dt, \tag{2.16}$$

where $dV = dAdx$ and A stands for the cross-sectional area. It is assumed that the material parameters as functions of spatial coordinates are symmetric with respect to the xz-plane. Thereby, terms linear with respect to the y-coordinate vanish upon integration. The variation of the work done by external forces can be expressed as

$$\int_{t_0}^{t_1} \delta W_1 dt = \int_{t_0}^{t_1} \left(\int_0^L q\delta w dx + Q_1 \delta w|_0^L + M_1 \delta w'|_0^L + M_2 \delta w''|_0^L \right) dt. \tag{2.17}$$

We note that in case of axial loadings, the x-component of the displacement field is enriched by the corresponding variable u as $u_x = u - yw'$. However, as within classical elasticity theory, the higher-order differential equations with respect to u and w remain uncoupled.

Let us next consider the beam structure composed of three layers – two facesheets and a core – which is called a sandwich structure as depicted in Fig. 1. Thus, it is assumed that all material parameters are piecewise constant functions across the thickness as shown in Fig. 1c for Young's modulus. By substituting (2.15)–(2.17) into (2.1), one can derive the differential equation in the form

$$-(\overline{EI} + \overline{EAg^2})w^{(4)} + \overline{EIg^2}w^{(6)} + q = \overline{\rho A}\ddot{w} - (\overline{\rho I} + 2\overline{\rho A\gamma^2})\ddot{w}'' + \overline{\rho I\gamma^2}\ddot{w}^{(4)}, \quad \forall x \in (0, L) \tag{2.18}$$

with the essential – Dirichlet type – boundary conditions (BCs) (left column) as well as the natural – Neumann type – BCs (right column) defined as

$$w = w_0 \quad \text{or} \quad Q_1 = -(\overline{EI} + \overline{EAg^2})w''' + \overline{EIg^2}w^{(5)} + (\overline{\rho I} + 2\overline{\rho A\gamma^2})\ddot{w}' - \overline{\rho I\gamma^2}\ddot{w}^{(3)}, \tag{2.19}$$

$$w' = w_1 \quad \text{or} \quad M_1 = (\overline{EI} + \overline{EAg^2})w'' - \overline{EIg^2}w^{(4)} + \overline{\rho I\gamma^2}\ddot{w}'', \tag{2.20}$$

$$w'' = w_2 \quad \text{or} \quad M_2 = \overline{EIg^2}w''' \quad \text{at } x = 0, L, \tag{2.21}$$

where

$$\begin{aligned} \overline{EI} &= E_f I_f + E_c I_c, \quad \overline{EIg^2} = E_f I_f g_f^2 + E_c I_c g_c^2, \quad \overline{EAg^2} = E_f A_f g_f^2 + E_c A_c g_c^2, \\ \overline{\rho I} &= \rho_f I_f + \rho_c I_c, \quad \overline{\rho I\gamma^2} = \rho_f I_f \gamma_f^2 + \rho_c I_c \gamma_c^2, \\ \overline{\rho A} &= \rho_f A_f + \rho_c A_c, \quad \overline{\rho A\gamma^2} = \rho_f A_f \gamma_f^2 + \rho_c A_c \gamma_c^2. \end{aligned} \tag{2.22}$$

Subscripts f and c stand for the facesheet and core materials, respectively.

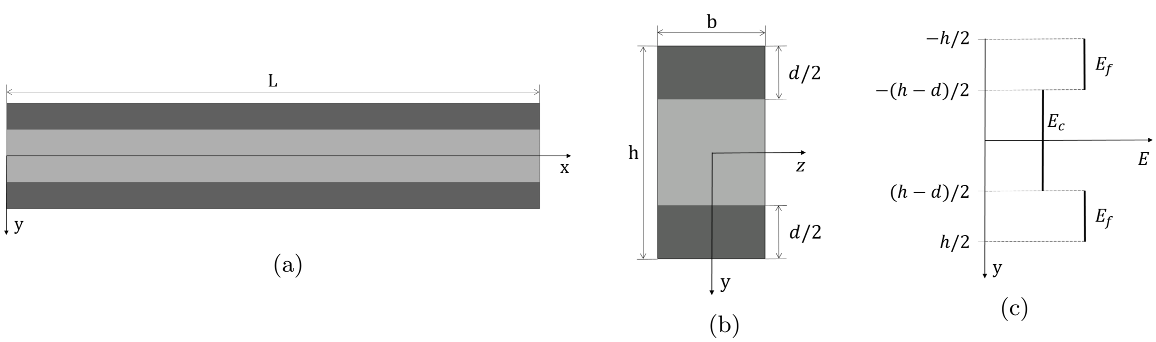

Figure 1: Long prismatic body: (a) in the xy-plane and (b) yz-plane. (c) Distribution of Young's modulus across the thickness.

It is worth noting that within the kinematical assumptions (2.13) the derived generalized sandwich beam model corresponds to the so-called engineering theory of sandwich beams. The strong form (2.18)– (2.21) stays valid for multi-layer and functionally graded beam structures as well. The overlined terms are defined analogously to the expressions in (2.22). In case of homogeneous beams, the model reduces to the corresponding one in [25].

2.3 Generalized Timoshenko model for sandwich beams

Let us derive the Timoshenko beam bending model for the prismatic body described in section 2.2. According to the kinematic assumptions of the Timoshenko model, the components of the displacement vector can be written as

$$u_x = -y\beta(x, t), \quad u_y = w(x, t), \quad u_z = 0, \tag{2.23}$$

where along with deflection $w(x,t)$ we introduce rotation $\beta(x,t)$ of a beam cross section around the neutral axis.

By following the assumptions made in Subsection 2.1, one can write the non-zero components of the stress tensors required for further derivation of the strain energy:

$$\begin{gathered}\tau_{xx} = E\varepsilon_{xx}, \quad \tau_{xy} = \tau_{yx} = 2G\varepsilon_{xy}, \\ \mu_{xxx} = g^2 E\partial_x\varepsilon_{xx}, \quad \mu_{yxx} = g^2 E\partial_y\varepsilon_{xx}, \quad \mu_{xxy} = \mu_{xyx} = 2g^2 G\partial_x\varepsilon_{xy},\end{gathered} \tag{2.24}$$

where $G = E/(2(1+\nu))$ stands for the shear modulus as usual.

By using the kinematic assumptions (2.23), one can rewrite expression (2.5) for the kinetic energy variation as follows (analogously to (2.15)):

$$\delta\int_{t_0}^{t_1}\int_{\Omega} T d\Omega dt = -\int_{t_0}^{t_1}\int_0^L\int_A \rho\left(\ddot{w}\delta w + (y^2+\gamma^2)\ddot{\beta}\delta\beta + \gamma^2\ddot{w}'\delta w' + y^2\gamma^2\ddot{\beta}'\delta\beta'\right) dV dt. \tag{2.25}$$

Similarly, with the aid of (2.23) and (2.24), the variation of the strain energy (2.7) transforms into (on the analogy of (2.16)):

$$\begin{aligned}\delta\int_{t_0}^{t_1}\int_{\Omega} W d\Omega dt = \int_{t_0}^{t_1}\int_0^L\int_A \Big(& E(y^2+g^2)\beta'\delta\beta' + Eg^2y^2\beta''\delta\beta'' \\ & + G(w'-\beta)(\delta w'-\delta\beta) + g^2G(w''-\beta')(\delta w''-\delta\beta')\Big) dV dt.\end{aligned} \tag{2.26}$$

The variation of work done by external forces (2.17) undergoes a change as well:

$$\int_{t_0}^{t_1}\delta W_1 dt = \int_{t_0}^{t_1}\left(\int_0^L (q\delta w + m\delta\beta)\, dx + Q_1\delta w|_0^L + Q_2\delta w'|_0^L + M_1\delta\beta|_0^L + M_2\delta\beta'|_0^L\right) dt. \tag{2.27}$$

Substituting equations (2.25)–(2.27) into the Hamilton's principle (2.1) implies governing equation of an isotropic Timoshenko sandwich beam with material parameters changing along the thickness direction:

$$\overline{GA}(w''-\beta') - \overline{GAg^2}(w''''-\beta''') + q = \overline{\rho A}\ddot{w} + \overline{\rho A\gamma^2}\ddot{w}'' \tag{2.28}$$

$$\overline{EI}\beta'' - \overline{EIg^2}\beta'''' + \overline{GA}(w'-\beta) - \overline{GAg^2}(w'''-\beta'') + \overline{EAg^2}\beta'' + m = \overline{\rho I}\ddot{\beta} - \overline{\rho I\gamma^2}\ddot{\beta}'' + \overline{\rho A\gamma^2}\ddot{\beta}, \tag{2.29}$$

for all $x \in (0,L)$ as well as the boundary conditions at $x = 0, L$:

$$w = w_0 \quad \text{or} \quad Q_1 = \overline{GA}(w'-\beta) - \overline{GAg^2}(w'''-\beta'') + \overline{\rho A\gamma^2}\ddot{w}', \tag{2.30}$$

$$w' = w_1 \quad \text{or} \quad Q_2 = \overline{GAg^2}(w''-\beta'), \tag{2.31}$$

$$\beta = \beta_0 \quad \text{or} \quad M_1 = \overline{EI}\beta' - \overline{EIg^2}\beta''' - \overline{GAg^2}(w''-\beta') + \overline{EAg^2}\beta' + \overline{\rho I\gamma^2}\ddot{\beta}', \tag{2.32}$$

$$\beta' = \beta_1 \quad \text{or} \quad M_2 = \overline{EIg^2}\beta''. \tag{2.33}$$

For the sandwich structure described in Subsection 2.2, the overlined parameters in (2.28)–(2.33) related to shear deformation are defined as follows:

$$\overline{GA} = \kappa(G_fA_f + G_cA_c), \quad \overline{GAg^2} = \kappa(G_fA_fg_f^2 + G_cA_cg_c^2), \tag{2.34}$$

while other parameters are defined as in (2.22). Shear correction factor κ is added according to [50]. In case of homogeneous beams, the model reduces to the corresponding one in [26].

3 Triangular lattice structure: homogenization via classical techniques

In this section, we consider a 2D triangular lattice structure presented in Fig. 2a made of isotropic material with Young's modulus $E = 2$ GPa, Poisson's ratio $\nu = 0.25$ and volume density $\rho = 1040$ kg/m^3. The effective classical mechanical properties are defined according to [51]. It is assumed that the effective homogenized continuum is governed by the generalized Hooke's law for orthotropic materials. The main homogenization steps based on classical homogenization techniques and finite element simulations are highlighted below.

At first, we choose the representative volume element (RVE) as depicted in Fig. 2b with dimensions given in Table 1. Next, we solve two problems by stretching RVE in the directions of axes x_1 and x_2 by setting the following boundary conditions: $u_1 = \pm u_1^\circ/2$ at $x_1 = \pm h_1/2$ and $u_2 = 0$ at $x_2 = \pm h_2/2$, for problem (1), and $u_1 = 0$ at $x_1 = \pm h_1/2$ and $u_2 = \pm u_2^\circ/2$ at $x_2 = \pm h_2/2$, for problem (2).

The effective material properties are defined by resolving the equations of the generalized Hooke's law with respect to two Young's moduli E_1^* and E_2^* and two Poisson's ratios ν_{12}^* and ν_{21}^*:

$$\begin{cases} E_1^* \varepsilon_{11}^\circ &= \langle \tau_{11}^{(1)} \rangle - \nu_{12}^* \langle \tau_{22}^{(1)} \rangle \\ 0 &= \langle \tau_{22}^{(1)} \rangle - \nu_{21}^* \langle \tau_{11}^{(1)} \rangle \\ 0 &= \langle \tau_{11}^{(2)} \rangle - \nu_{12}^* \langle \tau_{22}^{(2)} \rangle \\ E_2^* \varepsilon_{22}^\circ &= \langle \tau_{22}^{(2)} \rangle - \nu_{21}^* \langle \tau_{11}^{(2)} \rangle \end{cases}, \tag{3.35}$$

where $\varepsilon_{11}^\circ = u_1^\circ/h_1$ and $\varepsilon_{22}^\circ = u_2^\circ/h_2$. The superscripts (1) and (2) indicate that the corresponding strains and stresses are defined upon solving problems (1) and (2), respectively. The averaging procedure is defined as

$$\langle \boldsymbol{\tau} \rangle = \frac{1}{V} \int\limits_V \boldsymbol{\tau} dV, \tag{3.36}$$

where $V = h_1 h_2$ denotes the RVE volume. The effective volume density is defined as $\rho^* = \rho V_m/V$, where V_m stands for the volume occupied by the base material with respect to RVE. For more details, one can consult [51].

The values of the effective material constants are listed in Table 1. As can be seen, the mechanical properties in two directions exactly coincide, which allows us to conclude that such a triangular lattice structure behaves as an isotropic material, at least in the classical sense. The value of Poisson's ratio is close to the theoretical estimation $\nu = 1/3$ based on the discrete spring model in [52].

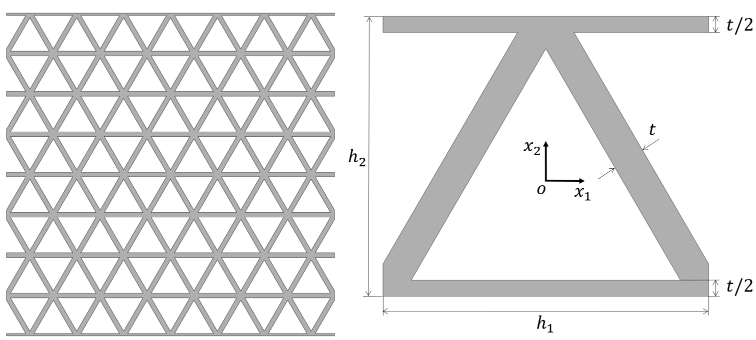

(a) (b)

Figure 2: (a) 2D triangular lattice structure. (b) Representative volume element.

Table 1: Dimensions and effective properties of RVE.

h_1, [mm]	h_2, [mm]	t, [mm]	E_1^*, [MPa]	E_2^*, [MPa]	ν_{12}^*	ν_{21}^*	ρ^*, [kg/m^3]
5	4.33	0.5	246.7	246.7	0.335	0.335	329.1

4 Triangular lattice structure: size-dependent mechanical response in bending, buckling and vibration

In this section, we investigate the size-dependent mechanical response of a 2D triangular lattice structure by considering three problem settings, namely, static bending, static buckling and transversal vibrations. It is worth noting that triangular lattices are stretching dominated structures [53], this fact remains valid for the selected test settings as well. Thus, for the corresponding homogenized continuum, rotational degrees of freedom (DOFs) associated to the bending of the struts are not active, which excludes the higher-order continuum models associated with rotational DOFs from consideration.

At first, we compose a lattice strip with thickness $a = 4.33$ mm and length l as shown in Fig. 3a by copying a single RVE (shown in Fig. 2b) along the x-axis and then, by duplicating it in the x- and y-directions, we produce strip specimens of length $L = Nl$ and thickness $h = Na$, $N = 1, 2, 3, \ldots$, such that the ratio of the strip thickness to the length is kept constant $L/h = l/a$. These specimens are called type 1. Next, in order to make the outer struts of the same thickness t (see Fig. 2b) as the inner ones, we attach a thin layer with thickness $d/2$ made of the same material to the upper and lower sides of each strip specimen of type 1 as shown in Fig. 3b. The built samples are called type 2.

For specimens of type 2, the outer layers (dark grey) act as facesheets, whereas the inner lattice structure (light grey) forms the core. The facesheets are modelled by a classical material, while the sandwich core is replaced by an effective strain gradient continuum with the classical material parameters $E = E_1^*$ and $\rho = \rho^*$ listed in Table 2. The given values for the intrinsic length scales g and γ are defined in the next subsections. Specimens of type 1 are assumed to be sandwich beams with zero facesheet thickness, i.e, they are modelled as homogeneous strain-gradient beams with material parameters associated to the sandwich core. Numerical experiments are accomplished via a commercial finite element software Abaqus (standard 2D solid elements and modified beam elements).

Table 2: List of sandwich material parameters.

	E, [MPa]	ρ, [kg/m^3]	g, [mm]	γ, [mm]
Facesheet	2000	1040	0	0
Core	246.7	329.1	1.57	2.51

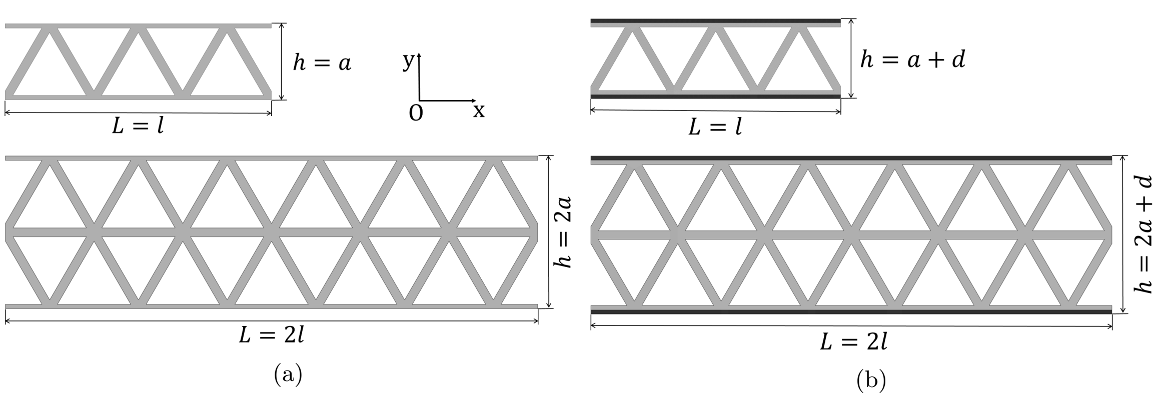

Figure 3: Lattice structure strips (a) of type 1 and (b) type 2 made of the same base material depicted by light grey or dark grey.

4.1 Bending rigidity

Let us consider a static Bernoulli–Euler bending problem (eliminating the right hand side terms in (2.18)) without a body load ($q = 0$). The higher-order term in the left hand side is neglected as well. Namely, in [25] it is shown that, essentially, the higher-order term plays a role in capturing and describing boundary layer effects. In the present work, our focus lies on the global response of the structure which with reliable accuracy can be modelled by the reduced strain gradient model. For static regimes, the strong formulation (2.18)–(2.21) then reduces to

$$(\overline{EI} + \overline{EAg^2})w^{(4)} = 0, \quad \forall x \in (0, L) \tag{4.37}$$

$$Q_1 = -(\overline{EI} + \overline{EAg^2})w''' \quad \text{or} \quad w = w_0, \tag{4.38}$$

$$M_1 = (\overline{EI} + \overline{EAg^2})w'' \quad \text{or} \quad w' = w_1,\ x = 0, L. \tag{4.39}$$

This model coincides with the so-called modified couple-stress model [25]. For a cantilever beam bended by a transversal load at the free end (see Fig. 4a), the boundary conditions simply read as $w(0) = 0$, $w'(0) = 0$, $Q_1(L) = F$ and $M_1(L) = 0$ resulting in the following expression for the deflection at the free end $x = L$:

$$w_{gr}^{BE} = \frac{FL^3}{3(\overline{EI} + \overline{EAg^2})}. \tag{4.40}$$

For rectangular cross-sections, the second moments of area are $I = bh^3/12,\ I_c = b(h-d)^3/12,$ $I_f = I - I_c$. The corresponding normalized bending rigidity takes the form

$$\frac{D}{D_0} = 1 + 12\frac{g^2}{h^2}(1 - d/h) + \frac{\Delta E}{E_c}(1 - (1 - d/h)^3), \tag{4.41}$$

where $\Delta E = E_f - E_c$. In case of a homogeneous beam ($d = 0$), it holds that

$$\frac{D}{D_0} = 1 + 12\frac{g^2}{h^2}, \tag{4.42}$$

where $D_0 = F/w_{cl}^{BE}$ denotes the bending rigidity within the classical Bernoulli–Euler model and $w_{cl}^{BE} = FL^3/(3E_cI)$ stands for the deflection at point $x = L$ within the classical elasticity theory ($g = 0$).

For the numerical simulations, the problem setting is the following: The left end ($x = 0$) is fixed, the free end ($x = L$) is loaded by a concentrated force F acting in the y-direction as shown in Fig. 4a. The length to thickness ratio is fixed to $l/a = 20.8$ for all samples. The truss is modelled as a 2D domain discretized by a fine enough mesh of quadrilateral elements (CPS4 type in Abaqus). The bending rigidity is calculated as the ratio of the applied force to the deflection w^{FE} at $y = 0,\ x = L$ as $D = F/w^{FE}$.

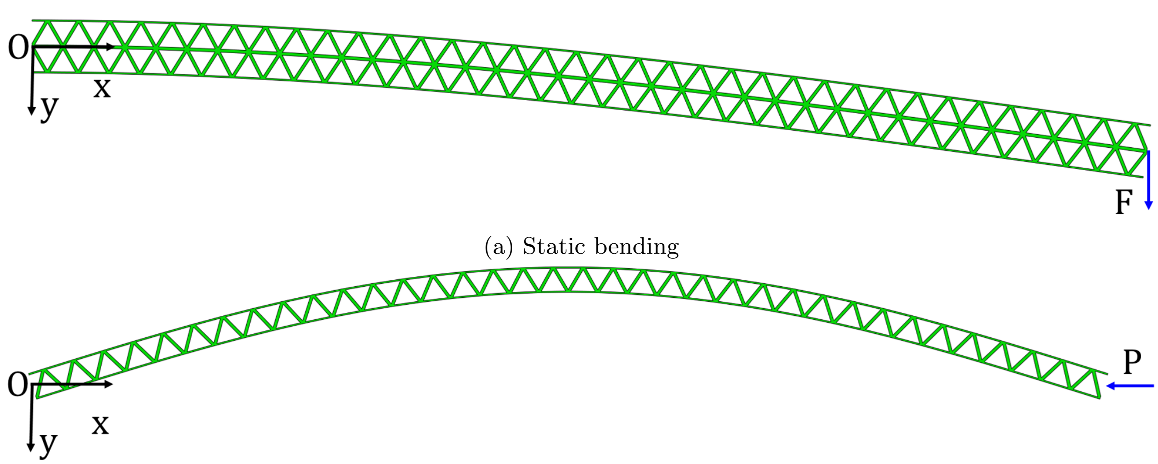

(a) Static bending

(b) Static buckling

Figure 4: Problem settings for the computational analysis. (a) Static bending of a clamped strip with $h = 8.66$ mm and $L = 180$ mm. (b) Static buckling of a simply supported strip with $h = 4.33$ mm and $L = 180$ mm.

The normalized bending rigidity against the beam thickness is plotted in Fig. 5. The blue dots correspond to the numerical simulation of static bending. The horizontal black line stands for the classical bending rigidity which stays at level one. In Fig. 5a, the red line is prescribed by expression (4.42) valid for the homogeneous beams (specimens of type 1). A plot fitting for the blue dots and the red line calibrates the intrinsic structural length scale parameter to $g = 1.57$ mm. It can be seen that after the calibration, for coarse microstructures ($N = 1, .., 4$) in which the size of triangles is comparable to the thickness of the beam, the generalized model of Subsection 2.2 is necessary in order to describe the size-dependent bending phenomenon. For dense microstructures ($N \geq 16$) in which the triangular microstructure becomes unnoticeable and the material can be hence regarded as homogeneous, the classical bending rigidity is retrieved.

The behaviour of sandwich beams (specimens of type 2) is represented in Fig. 5b. The red line is governed by expression (4.41). It can be seen that the behaviour of the specimens of type 2 (see Fig. 3b) is again perfectly captured by the strain gradient sandwich beam model derived in Subsection 2.2.

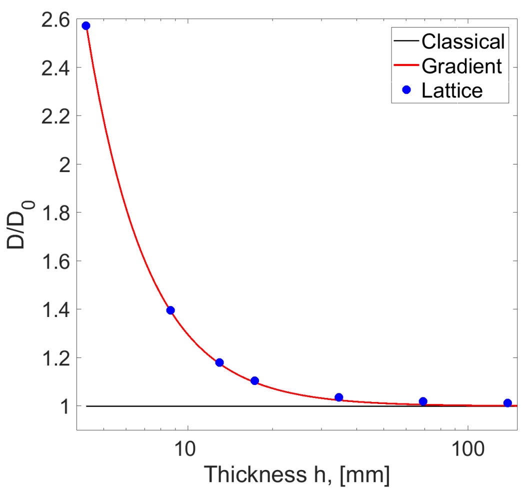

(a)

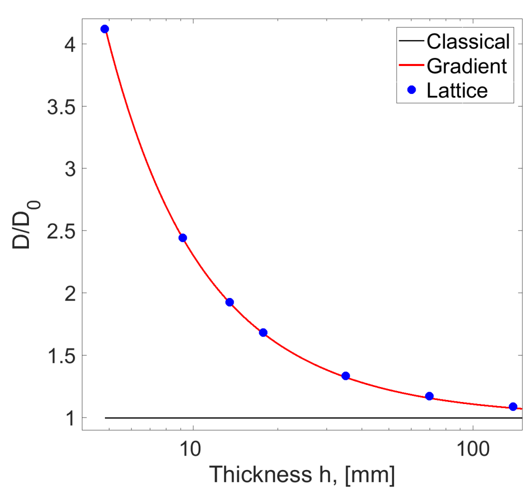

(b)

Figure 5: Normalized bending rigidity (a) for the homogeneous beams (specimens of type 1) and (b) for the sandwich beams (specimens of type 2).

4.2 Critical buckling load

For static linear buckling, the variation of the work done by external forces (2.17) is enriched by a term corresponding to the work of a compressive force P as [18]

$$\delta W_1^P = \delta W_1 + \int_0^L P w' \delta w' dx. \tag{4.43}$$

The corresponding strong formulation of the problem is of the form

$$(\overline{EI} + \overline{EAg^2}) w^{(4)} - \overline{EIg^2} w^{(6)} + P w'' = q, \quad \forall x \in (0, L) \tag{4.44}$$

$$w = w_0 \quad \text{or} \quad Q^P = -P w' + Q_1, \tag{4.45}$$

$$w' = w_1 \quad \text{or} \quad M_1 = (\overline{EI} + \overline{EAg^2}) w'' - \overline{EIg^2} w^{(4)}, \tag{4.46}$$

$$w'' = w_2 \quad \text{or} \quad M_2 = \overline{EIg^2} w^{(3)}, \ x = 0, L. \tag{4.47}$$

As in the previous subsection, we neglect the higher-order term and eliminate distributed forces ($q = 0$). For the simply supported case, $w(0) = w(L) = 0$, $M_1(0) = M_1(L) = 0$, the critical buckling loads are given as

$$P = \frac{\pi^2 n^2}{L^2}(\overline{EI} + \overline{EAg^2}),\ \ n = 1, 2, 3, \dots \ . \tag{4.48}$$

For rectangular cross-sections, the normalized critical loads are expressed in the form

$$\frac{P}{P_0} = 1 + 12\frac{g^2}{h^2}(1 - d/h) + \frac{\Delta E}{E_c}(1 - (1 - d/h)^3) \tag{4.49}$$

which is valid for all eigenmodes. In case of homogeneous beams ($d = 0$), the normalized buckling loads are given as

$$\frac{P}{P_0} = 1 + 12\frac{g^2}{h^2}, \tag{4.50}$$

where $P_0 = \pi^2 n^2 E_c I/L^2$ denotes the critical load of the classical elasticity model. It is notable that expressions (4.49) and (4.50) coincide with the corresponding expressions for the normalized bending rigidities (4.41) and (4.42), respectively.

For buckling analysis, for specimens of type 1 we choose thin beams and set $L/h = 41.6$. The normalized values of the first buckling load calculated via numerical simulations are shown in Fig. 6 by blue dots. In Fig. 6a, the results correspond to strips of type 1. The red line, governed by (4.50), stands for the homogeneous generalized beam model. In Fig. 6b, representing the sandwich beam case, the red line is defined by (4.49).

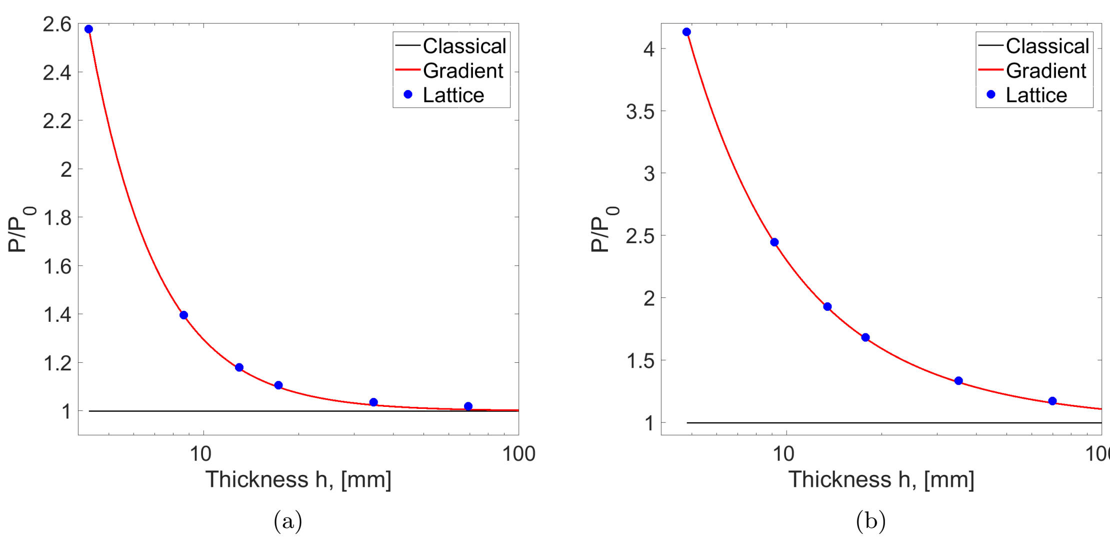

Figure 6: Normalized first buckling load ($n = 1$) as a function of strip thickness with $L/h = 41.6$ (a) for the homogeneous beams (specimens of type 1) and (b) for the sandwich beams (specimens of type 2).

4.3 Eigenanalysis

For beams of infinite length, we seek for a wave form solution as $w(x, t) = W_0 e^{-i(kx - \omega t)}$, where i is the imaginary unit, k stands for the wavenumber, ω denotes the angular frequency and W_0 is the wave amplitude. In case of long waves (low frequencies), we neglect the higher-order terms $\overline{EIg^2}w^{(6)}$ and $\overline{\rho I\gamma^2}\ddot{w}^{(4)}$ in (2.18), which eliminates the highest degrees of wave number k in the dispersion relation $\omega = \omega(k)$. For the reduced strain gradient elastic beam model, the dispersion relation is given as

$$\omega = k^2 \sqrt{\frac{\overline{EI} + \overline{EAg^2}}{\overline{\rho A} + (\overline{\rho I} + 2\overline{\rho A\gamma^2})k^2}}. \tag{4.51}$$

For rectangular cross-sections, dispersion relation (4.51) is rewritten as

$$\omega = k^2\sqrt{\frac{E_c}{\rho_c}}\sqrt{\frac{1+12\dfrac{g^2}{h^2}(1-d/h)+\dfrac{\Delta E}{E_c}(1-(1-d/h)^3)}{12(1+\dfrac{\Delta\rho}{\rho_c}d/h)/h^2+(1+24\dfrac{\gamma^2}{h^2}(1-d/h)+\dfrac{\Delta\rho}{\rho_c}(1-(1-d/h)^3))k^2}}. \tag{4.52}$$

In case of homogeneous beams ($d = 0$), the dispersion relation degenerates into the expression

$$\omega = k^2\sqrt{\frac{E_c}{\rho_c}}\sqrt{\frac{1+12g^2/h^2}{12/h^2+(1+24\gamma^2/h^2)k^2}}. \tag{4.53}$$

For the simply supported case, $w(0) = w(L) = 0$, $M_1(0) = M_1(L) = 0$, the wave number values are explicitly defined as $k_n = \pi n/L$, $n = 1, 2, 3, \dots$.

Let us at first consider the lattice specimens of type 1 with $L/h = 41.6$ and the corresponding samples of type 2. Side edges ($x = 0$ and $x = L$) are constrained in a way corresponding to a simply supported beam. By varying the strip thickness, we compare the first frequency of the triangular lattice structure strips with the corresponding first eigenvalue predicted by the classical and generalized beam models. For the specimens of type 1, the comparison is performed with respect to the analytical expression (4.53), whereas relation (4.52) is utilized for the samples of type 2. The comparison is presented in Fig. 7a for homogeneous beams and in Fig. 7b for sandwich beams. The first frequency ($n = 1$) is calculated by $f_1 = \omega/(2\pi)$. The classical model gives $f_1^{cl} = \pi\sqrt{E_c h^2/(12\rho_c)}/(2L^2)$.

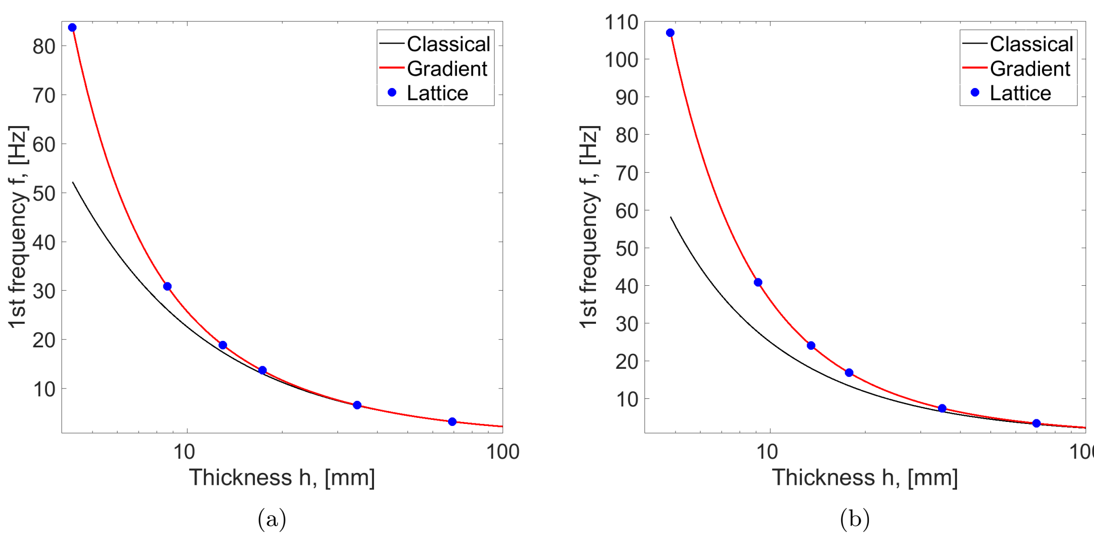

Figure 7: The first frequency against the strip thickness (a) for the homogeneous beams (specimens of type 1) and (b) for the sandwich beams (specimens of type 2).

Next, for a specimen of type 1 with $h = 4.33$ mm and $L = 720$ mm ($L/h = 166.3$) and for the corresponding sample of type 2, the eigenfrequency spectrum as a function of (angular) wavenumber k is represented in Fig. 8 (blue circles). In Fig. 8a, the black solid line corresponds to the classical beam model (eq. (4.53) with $g = \gamma = 0$), the green solid line represents the strain gradient beam model without the higher-order inertia term (eq. (4.53) with $\gamma = 0$), the red solid line relates to the gradient-elastic beam model accounting for the first velocity gradient (eq. (4.53) with $g = 1.57$ mm, $\gamma = 2.51$ mm). For small wavenumbers, we report that dispersion relation (4.53) based on the strain gradient beam model perfectly matches the experimental eigenvalues (extracted upon numerical simulations with fine-scale FE models for the lattice specimen of type 1).

In Fig. 8b, concerning the sandwich lattice structure, we observe that the Bernoulli–Euler model (BE) of sandwich beams (giving the dispersion relation in form (4.52) and represented by the red solid curve) fails to describe the dynamic response of the sandwich lattice structure (sample of type 2). The reason is that normal fibres of the beam axis do not remain as normals during the deformation for wavenumbers larger than $k^* \approx 0.08$ r/mm. In the next section, it is shown that the generalized Timoshenko sandwich beam model (T) is capable of capturing such effect (as can be seen already in Fig. 8b).

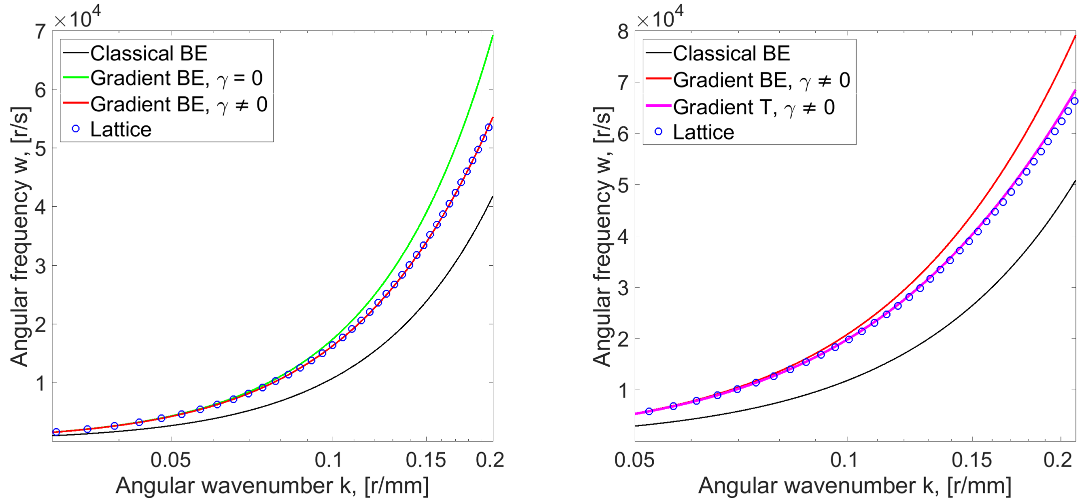

(a) (b)

Figure 8: Dispersion relations (a) for the homogeneous beam (sample of type 1) and (b) for the sandwich beam (sample of type 2).

5 Timoshenko model versus Bernoulli–Euler model

Let us define the problem of Subsection 4.1 for the Timoshenko beam model. Equations for the static case of a sandwich Timoshenko beam in the framework of gradient elasticity can be obtained by omitting the right hand side terms in (2.28)–(2.29):

$$\begin{gathered}\overline{GA}(w'' - \beta') - \overline{GAg^2}(w'''' - \beta''') + q = 0,\\ \overline{EI}\beta'' + \overline{GA}(w' - \beta) - \overline{GAg^2}(w''' - \beta'') + \overline{EAg^2}\beta'' + m = 0, \quad \forall x \in (0, L).\end{gathered} \tag{5.54}$$

The boundary conditions (2.30)–(2.33) can be rewritten in the form

$$w = w_0 \quad \text{or} \quad Q_1 = \overline{GA}(w' - \beta) - \overline{GAg^2}(w''' - \beta''), \tag{5.55}$$

$$w' = w_1 \quad \text{or} \quad Q_2 = \overline{GAg^2}(w'' - \beta'), \tag{5.56}$$

$$\beta = \beta_0 \quad \text{or} \quad M_1 = \overline{EI}\beta' - \overline{GAg^2}(w'' - \beta') + \overline{EAg^2}\beta'. \tag{5.57}$$

Note that here, similarly to the case of Bernoulli–Euler beams, we omit the higher-order terms in (2.29), (2.32) and (2.33).

For a cantilever beam affected by a transversal load at the free end, the boundary conditions can be written as follows: $w(0) = 0$, $\beta(0) = 0$, $Q_2(0) = 0$, $Q_1(L) = F$, $M_1(L) = 0$, $Q_2(L) = 0$. Deflection at the right end ($x = L$) is equal to

$$w_{gr}^T = \frac{FL(L^2\overline{GA}/3 + \overline{EI} + \overline{EAg^2})}{\overline{GA}(\overline{EI} + \overline{EAg^2})}, \tag{5.58}$$

which for the homogeneous beam can be simplified as follows:

$$w_{gr}^T = \frac{FL(L^2\kappa GA/3 + EI + EAg^2)}{\kappa GAE(I + Ag^2)}, \tag{5.59}$$

with $\kappa = 0.85$ in case of rectangular cross-sections [50].

It is a well known fact that the Bernoulli–Euler beam model is not able to describe bending of thick beams unlike the Timoshenko model. This fact is next shown to be valid for the case of lattice beams as well. Two models of extremely thick lattice beams are depicted in Fig. 9a for $L = 10$ mm, $h = 4.33$ mm and in Fig. 9b for $L = 15$ mm, $h = 4.33$ mm. Bending results for beams obtained by replicating these two specimens (with $L/h = 2.31$ and $L/h = 3.46$) are represented in Figure 10a. It can be seen that according to the Bernoulli–Euler model (green line) the normalized bending rigidity is not sensitive to the l/a-ratio, whereas the Timoshenko model (red lines) shows a good correlation with the fine-scale simulations (blue dots).

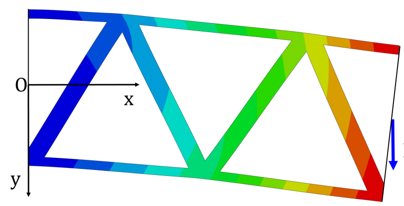

(a) $L/h = 2.31$

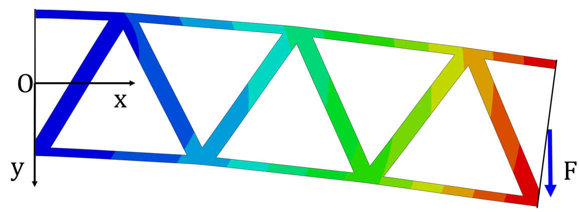

(b) $L/h = 3.46$

Figure 9: Static bending of clamped thick lattice structure strips (specimens of type 1) with $h = 4.33$ mm and (a) $L = 10$ mm, (b) $L = 15$ mm.

Figure 10b demonstrates the advantage of the Timoshenko beam model (T) over the Bernoulli–Euler model (BE) for a case of sandwich beams with length to thickness ratio $l/a = 5.77$. However, for smaller values of l/a, both models fail to describe the bending behaviour properly (as shown in Fig. 10b for $l/a = 2.31$). A visual analysis of the deformed state shows that the cross sections do not remain planar, which means that "engineering" sandwich beam theory is not sufficient and a more complicated theory (e.g., third order shear deformable beam theory) is required.

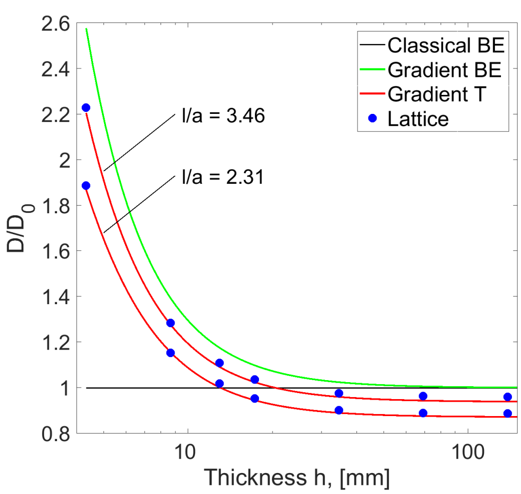

(a) $l/a = 2.31$ and $l/a = 3.46$

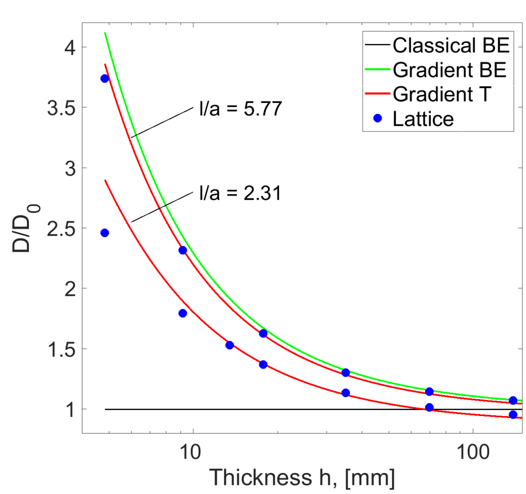

(b) $l/a = 5.77$

Figure 10: Normalized bending rigidity (a) for the homogeneous beams (specimens of type 1), (b) for the sandwich beams (specimens of type 2). Normalization is accomplished with respect to the bending rigidity within the corresponding classical Bernoulli–Euler beam model.

Let us finally turn our attention to the free vibration problem considered in Subsection 4.3 for Bernoulli–Euler beams. By assuming that the solution of the dynamic problem (equations (2.28) and (2.29) with the higher-order terms omitted) has the following form of the particular variable-separable functions:

$$w(x,t) = w(x)e^{-i\omega t}, \quad \beta(x,t) = \beta(x)e^{-i\omega t}, \tag{5.60}$$

one can derive a dispersion relation (expression for the eigenfrequency) in the form

$$\omega_{n_{1,2}} = \sqrt{\frac{-c_2 \mp \sqrt{c_2^2 - 4c_1c_3}}{2c_1}}, \tag{5.61}$$

with coefficients c_1, c_2 and c_3 defined as follows:

$$\begin{aligned} c_1 &= (\overline{\rho A} + \overline{\gamma^2 \rho A} k^2)(\overline{\rho I} + \overline{\gamma^2 \rho A}), \\ c_2 &= -k^2(\overline{GA} + \overline{g^2 GA} k^2)(\overline{\rho I} + \overline{\gamma^2 \rho A}) - (\overline{\rho A} + \overline{\gamma^2 \rho A} k^2)(\overline{GA} + \overline{g^2 GA} k^2 + \overline{EI} k^2 + \overline{g^2 EA} k^2), \\ c_3 &= k^4(\overline{GA} + \overline{g^2 GA} k^2)(\overline{EI} + \overline{g^2 EA}). \end{aligned} \tag{5.62}$$

Note that we do not discuss here the physicality of the second part of the eigen spectrum ω_{n_2} (with "+" sign in front of the inner square root in (5.61)) and consider only spectrum ω_{n_1}. In Fig. 8b, it can be seen that introducing the additional rotational degree of freedom of the Timoshenko beam model provides more accurate results for a wider range of eigenfrequencies (the magenta line crossing the majority of the blue circles) in comparison with the Bernoulli–Euler beam model (the red curve).

6 Application to auxetics

Let us consider a reentrant honeycomb structure [54] depicted in Fig. 11a (set to type A) being a representative of the so-called auxetics, i.e., materials with negative Poisson's ratio (see [55] for a review on auxetic materials). The geometrical characteristics are set to $a = 72.5$ mm, $b = 40$ mm, $t = 2.165$ mm and $\alpha = \pi/3$. By replacing solid struts with triangular lattice trusses as shown in Fig. 11b, we compose an auxetic structure of type B. The geometry of the triangular lattice trusses is defined in Section 3. The type C auxetic structure is obtained from type B by removing a part of the material from the fastenings as shown in Fig. 11c. The properties of the base material are $E = 2$ GPa, $\nu = 0.25$ and $\rho = 1040$ kg/m^3.

The effective elastic constants calculated through fine-scale FE modeling are listed in Table 3. The fine-scale FE models correspond to 2D FEM of 2D classical plane elasticity by standard Abaqus plane stress elements of type CPS4. The properties of type A auxetic are set as a reference. It can be seen that by modifying the "micro"-architecture of the reference auxetic, i.e., by utilizing hollow trusses, namely, triangular lattice trusses instead of solid ones (type B), it is possible to (i) reduce the mass of the structure by 23 %, (ii) dramatically increase the stiffness of the global structure (by 147 % and 163 % for E_x and E_y, respectively) with admissible reduction in Poisson's ratios (by 19 % and 8 % for ν_{xy} and ν_{yx}, respectively). By making fastenings lighter (type C), the mass of the global structure is reduced by 33 % with a similar reduction in Poisson's ratios, which makes the structure less stiff compared to the auxetic of type B, however.

It should be noted that the reentrant honeycomb structures in Figs. 11a–11c are bending-dominated in the sense that the bending part of the accumulated energy of each strut is essentially higher than the stretching part of the energy. In Subsection 4.1, it has been demonstrated that upon bending the triangular lattice strips demonstrate significant size dependency in bending rigidity, which, in fact, explains the considerable increase in Young's moduli of the architectured auxetic structures of types B and C (see the discussion in Subsection 7.1).

The fine-scale modeling, used for defining the effective elastic properties of the considered auxetic structures, is computationally extremely costly and hence the reduced modeling by structural beam elements is preferable (see Fig. 11d). For the auxetic structure of type A, the model reduction is straightforward since the use of standard beam elements of classical elasticity is sufficient. However, this approach is not valid for the auxetic structures of type B or C since the behaviour of lattice trusses is governed by generalized beam models as shown in Section 4. In general, the generalized beam element formulation based on (2.18)–(2.21) is required (see [25]). For the reduced strain gradient beam formulation (4.37)–(4.39), the intrinsic structural length scale parameter g can be incorporated into standard FE analysis by endowing the classical beam elements with effective second moment of area $I_{eff} = I + g^2 A$ (coming from (4.37)). As a result, compared to the fine-scale 2D FEM approach the number of DOFs is reduced by factor 82, whereas the computational time is reduced by factor 17.

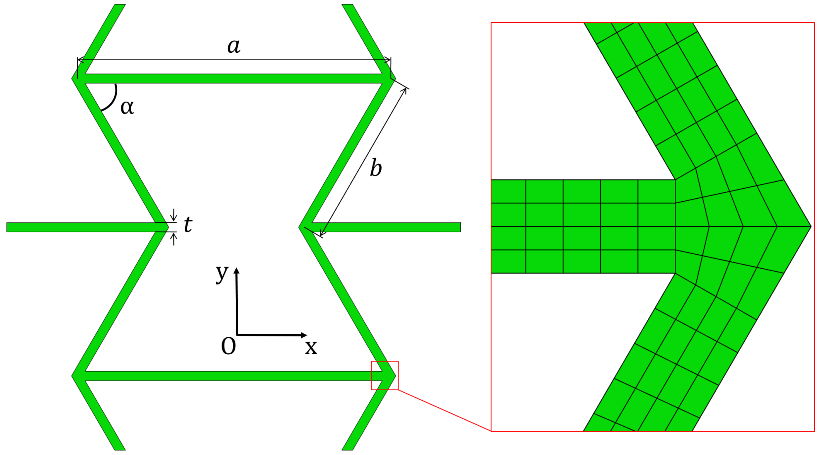

(a) Type A

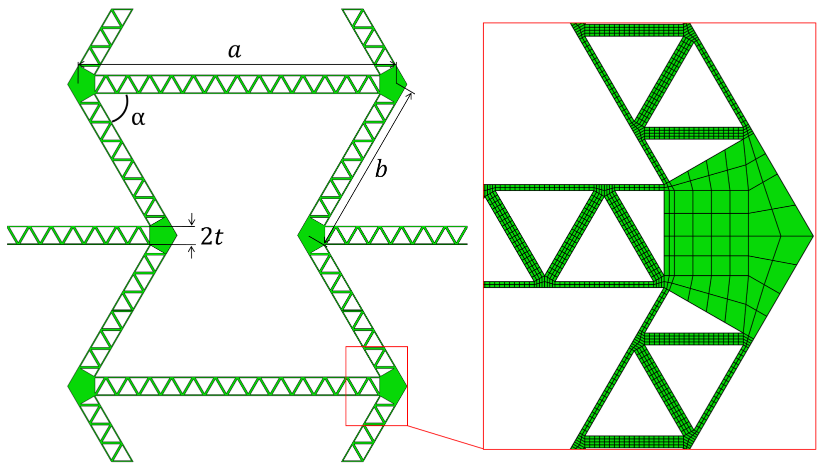

(b) Type B

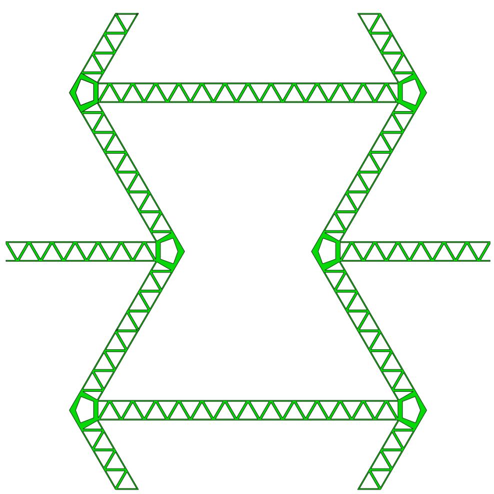

(c) Type C

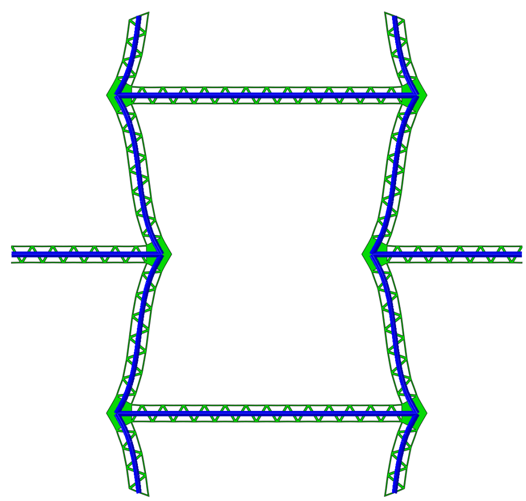

(d) Beam model

Figure 11: Auxetic material types made of (green) base material and the corresponding (blue) beam model. (a) Type A: solid struts (and finite elements of the fine-scale model). (b) Type B: struts with a triangular lattice microstructure with solid joints (and finite elements of the fine-scale model). (c) Type C: Type B struts with lightweight fastenings (finite elements of the fine-scale model not shown). (d) Deformed shape: reduced auxetic model by utilizing generalized beam elements (blue solid lines) against the Type B model (green).

The effective elastic properties of the auxetic structures defined by FEA of fine-scale and reduced models are compared in Table 4. It can be seen that the maximal deviation in values is 6.6 % (in E_x) for the type A structure and 4.8 % (in ν_{yx}) for the type B structure.

Table 3: List of auxetic effective properties.

Type	ρ, [kg/m^3]	ν_{xy}	ν_{yx}	E_x, [MPa]	E_y, [MPa]
A	92.5	-0.86	-1.13	0.76	1.04
B	71	-0.7	-1.04	1.88	2.73
C	62	-0.7	-1.06	1.57	2.39

Table 4: Comparison between fine-scale and reduced beam models of auxetic structures.

Elastic	Type A		Type B	
moduli	Fine-scale	Beam	Fine-scale	Beam
ν_{xy}	-0.86	-0.86	-0.7	-0.7
ν_{yx}	-1.13	-1.13	-1.04	-0.99
E_x, [MPa]	0.76	0.81	1.88	1.91
E_y, [MPa]	1.04	1.07	2.73	2.73

7 Discussions and conclusions

7.1 Mass-rigidity relationship and RVE scaling

At first, the mass-rigidity relationship is discussed. Let us consider a thin strip made of triangular lattice structure (described in Sections 3 and 4) with thickness $h = 4.33$ mm and the corresponding solid strips of thickness H made of the same material. The mechanical behaviour of the lattice and solid strips is captured, respectively, by the higher-order (strain gradient) and classical Bernoulli-Euler beam models. Relative mass M/M_s as well as relative bending rigidity D/D_s are expressed in the form

$$\frac{M}{M_s} = \frac{\rho^*}{\rho}\frac{h}{H}, \qquad \frac{D}{D_s} = \frac{E^*}{E}\Big(\frac{h}{H}\Big)^3(1 + 12\frac{g^2}{h^2}), \tag{7.63}$$

where characteristics M, D and h relate to the lattice structure strips, whereas M_s, D_s and H correspond to the solid strips.

The diagram of mass-rigidity relationship is shown in Fig. 12a. The relative mass is plotted with the blue line (defined by (7.63) (left)), while the red line stands for the relative bending rigidity (prescribed by (7.63) (right)). In Fig. 12a, it can be seen that by keeping the stiffness constant (relative bending rigidity $D/D_s = 1$) the lattice structure strip is lighter by 53.5% than the solid one, however occupying more space (thickness becomes larger by 47%) as shown in Fig. 13. For the case $h/H = 2$ (lattice structure is two times thicker than the solid one), the lattice structure beam is 2.52 times stiffer and lighter by 36.7% than the corresponding solid counterpart.

For comparison, the relative bending rigidity within the classical elasticity theory (utilized for the lattice strip) is represented by the black line (defined by (7.63) (right) with $g = 0$). It can be seen that neglecting the strain gradient effects leads to inappropriate modelling of the structure.

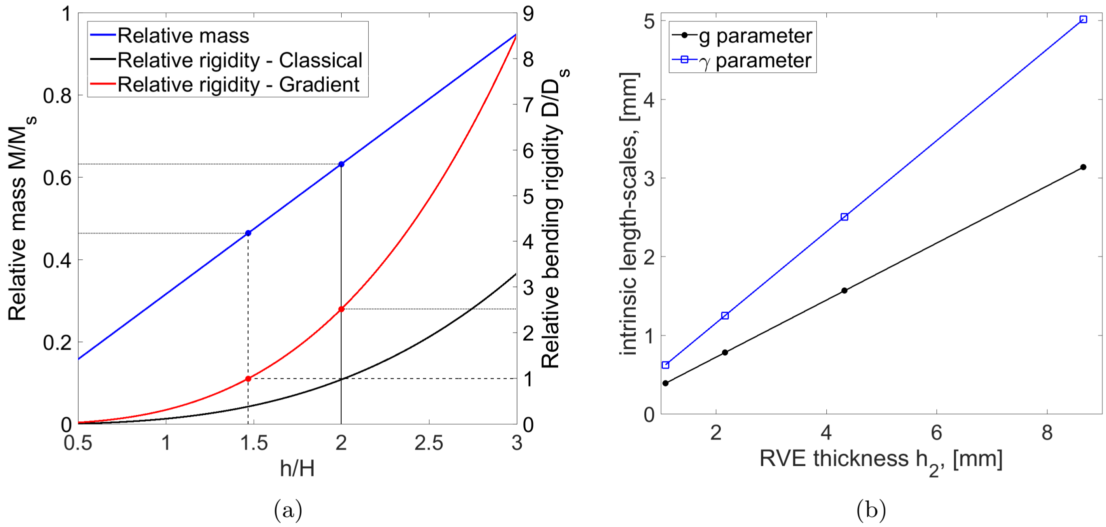

Figure 12: (a) Mass-rigidity relationship: relative mass M/M_s and bending rigidity D/D_0 against relative thickness h/H. (b) Intrinsic length scale parameters g and γ against thickness h_2 of the RVE.

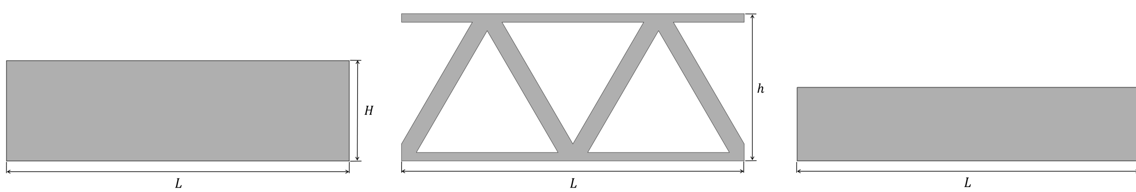

Figure 13: Representation of a lattice structure strip with $h = 4.33$ mm (middle) against its solid counterpart for $h/H = 1.47$ (left) and $h/H = 2$ (right).

Next, the effect of the RVE scaling on the effective material moduli is discussed. Upon scaling all geometric dimensions of the RVE are changed proportionally (by the same factor), meaning that the volume density of the effective material remains constant ($\rho^* = 329.1$ kg/m^3). By performing the homogenization procedure described in Section 3, it has been observed that classical elastic moduli E^* and ν^* are not sensitive to RVE scaling. By accomplishing the identification procedures described in Subsections 4.1 and 4.3, higher-order parameters g and γ are observed to obey linear dependence on RVE thickness h_2 as depicted in Fig. 12b. For all scaled RVEs, the ratios of the intrinsic length scale parameters to RVE thickness, namely, $g/h_2 = 0.36$ and $\gamma/h_2 = 0.58$ remain constant.

7.2 Effective moduli vs. RVE relative mass

Finally, the dependence of the effective moduli of the homogenized material on the relative RVE density are discussed. Different types of RVEs are represented in Fig. 14, where voids remain equilateral triangles. The corresponding classical elastic moduli are depicted in Fig. 15. It can be seen that for low-density RVEs, the effective Young's modulus (Fig. 15a) demonstrates linear dependence on relative density, which coincides with the estimated expression $E = E_s B(\bar{\rho}/100)^b$, where $E_s = 2$ GPa stands for Young's modulus of the solid and coefficients $B = 1/3$ and $b = 1$ correspond to a triangular lattice [53]. The effective Poisson's ratio (Fig. 15b) tends to the analytical value $\nu = 1/3$ [53] as the relative density of the RVE decreases.

The higher-order material parameters against the relative density of RVE are depicted in Fig. 16. For small values of the relative density, parameter g (Fig. 16a) depends linearly on $\bar{\rho}$ tending to value $g_0 \approx 1.7537$ in the limit $\bar{\rho} = 0$. As long as the relative density approaches value $\bar{\rho} = 100\%$, the higher-order elastic modulus g tends to value $g = 0$ corresponding to the classical elasticity theory.

Intrinsic length scale parameter γ follows a similar behaviour (Fig. 16b). In the region of high relative densities, the modulus undergoes rapid changes tending to zero as within classical continua.

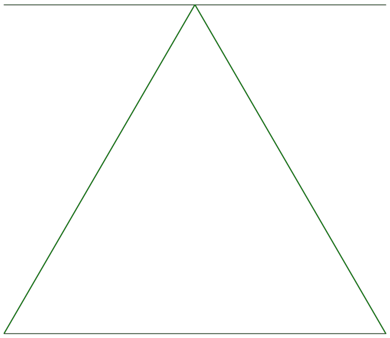

(a) $\bar{\rho} = 0.69\%$

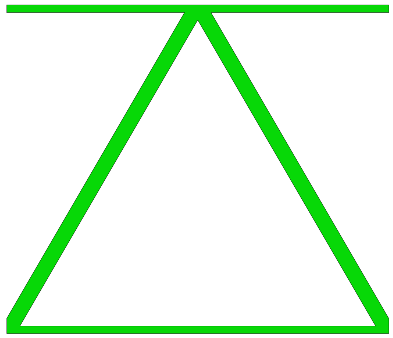

(b) $\bar{\rho} = 13.4\%$

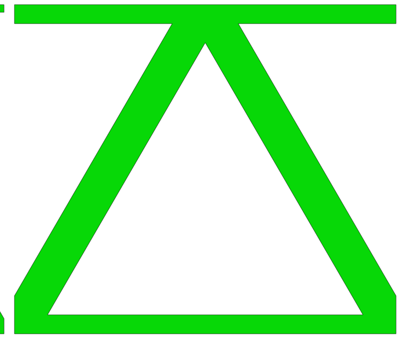

(c) $\bar{\rho} = 34.6\%$

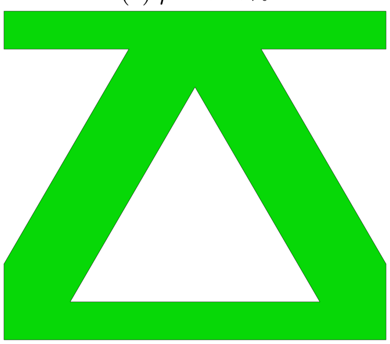

(d) $\bar{\rho} = 57.3\%$

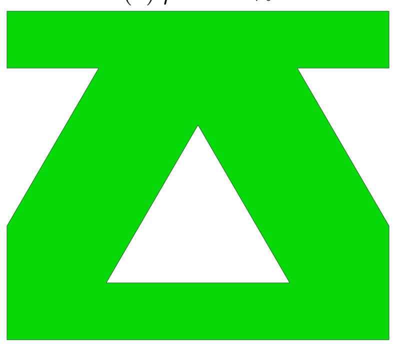

(e) $\bar{\rho} = 76.9\%$

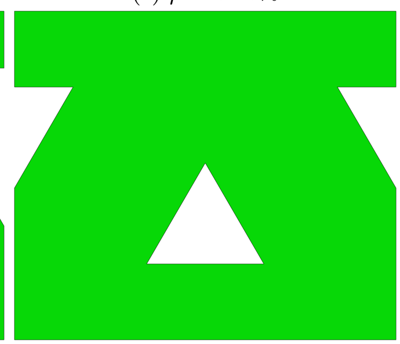

(f) $\bar{\rho} = 90.6\%$

Figure 14: RVEs with different relative densities $\bar{\rho}$

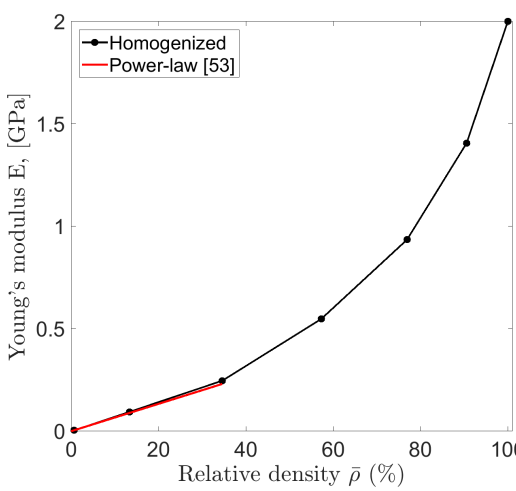

(a)

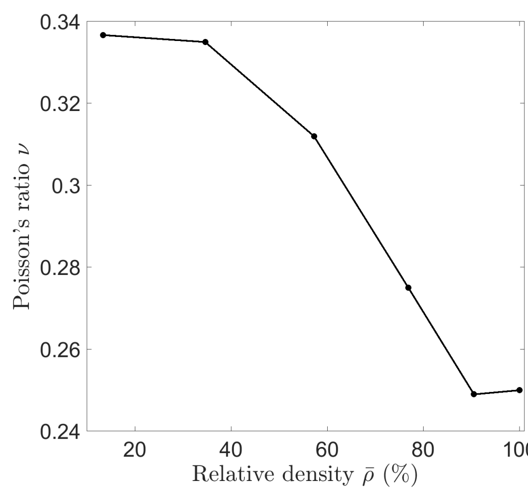

(b)

Figure 15: Effective classical elastic moduli against the relative density of RVE: (a) for Young's modulus and (b) for Poisson's ratio

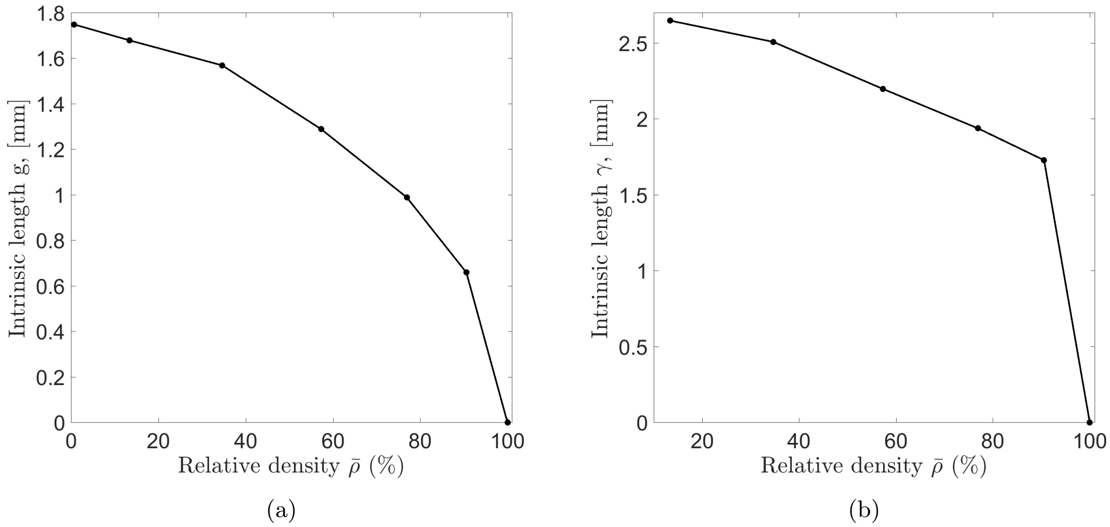

Figure 16: Higher-order material parameters against the relative density of RVE: (a) for intrinsic length scale parameter g and (b) for intrinsic length scale parameter γ.

7.3 Concluding remarks

This work should be considered as a contribution in the development and utility of generalized continuum theories in the context of engineering sciences and industrial applications. Accordingly, the main concluding remarks are summarized as follows:

1. The presented results prove the relevance and applicability of the beam models of the strain gradient elasticity theory with velocity gradient inertia terms.

2. Very good correlation between experimental (numerical) and analytical results provide, first, evidence on the strain gradient nature of lattice substructures and, second, calibration for both microstructural and micro-inertia length scale parameters.

3. The higher-order material moduli are shown to be independent of the problem type, boundary conditions and model formulations.

4. The strain gradient Bernoulli–Euler and Timoshenko models derived for sandwich beams are shown to be applicable for modeling beam structures composed of triangular lattices, which enables efficient modeling of complex structures and significantly reduces the computational costs in structural design and analysis phases.

5. For auxetic metamaterials formed by struts with a lattice microstructure (trusses), it is shown that, first, the elastic moduli of orthotropy of the metamaterial are improved by 147 % and 163 %, whereas mass is decreased by 23 %. Second, by replacing the fine-scale finite element model with the corresponding gradient-elastic beam element model the computational time is reduced by factor 17 and the number of degrees of freedom can be divided by 82, without loosing accuracy more than 5 %.

6. Finally, the mechanical properties for a full range of mass densities with a triangular lattice microstructure are reported providing a source for a design table to be utilized in practical engineering applications.

As a final conclusion, it can be stated that the demonstrations for sandwich beams and auxetics, in particular, propose pivotal information for practical applications and, in general, a set of new theoretical and computational tools for material and metamaterial design for materials and structures with a microstructure or microarchitecture.

Acknowledgements

Authors have been supported by Academy of Finland through the project *Adaptive isogeometric methods for thin-walled structures* (decision numbers 270007, 273609, 304122). Access and licenses for the commercial FE software Abaqus have been provided by CSC – IT Center for Science (www.csc.fi)

Appendices

A Higher-order beam model assumptions

For isotropic centrosymmetric materials, strain energy density (2.2) is explicitly expressed as [6, 12]

$$W = \frac{1}{2}\lambda\varepsilon_{ii}\varepsilon_{jj} + \mu\varepsilon_{ij}\varepsilon_{ij} + a_1\varepsilon_{iij}\varepsilon_{jkk} + a_2\varepsilon_{ijj}\varepsilon_{ikk} + a_3\varepsilon_{iik}\varepsilon_{jjk} + a_4\varepsilon_{ijk}\varepsilon_{ijk} + a_5\varepsilon_{ijk}\varepsilon_{kji}, \tag{A.64}$$

whereas constitutive relations (2.8) take the form

$$\tau_{pq} = \lambda\varepsilon_{ii}\delta_{pq} + 2\mu\varepsilon_{pq}, \tag{A.65}$$

$$\mu_{pqr} = a_1(\varepsilon_{iip}\delta_{qr} + \frac{1}{2}\varepsilon_{rii}\delta_{pq} + \frac{1}{2}\varepsilon_{qii}\delta_{pr}) + 2a_2\varepsilon_{pii}\delta_{qr} + a_3(\varepsilon_{iir}\delta_{pq} + \varepsilon_{iiq}\delta_{pr}) + 2a_4\varepsilon_{pqr} + a_5(\varepsilon_{rqp} + \varepsilon_{qpr}), \tag{A.66}$$

where $\varepsilon_{ijk} = \partial_i\varepsilon_{jk}$.

Along with the kinematical relations of (2.13), it is assumed that

$$\tau_{\alpha\beta} = 0, \quad \alpha, \beta = 2, 3, \tag{A.67}$$

which is used in the constitutive equation (A.65) in order to eliminate $\varepsilon_{\alpha\beta}$ leading to

$$\varepsilon_{yy} = \varepsilon_{zz} = -\frac{\lambda}{2(\mu+\lambda)}\varepsilon_{xx}, \quad \varepsilon_{yz} = 0. \tag{A.68}$$

By redefining the Lamé parameters as $\mu = E/2/(1+\nu)$ and $\lambda = \nu E/(1+\nu)/(1-2\nu)$, the classical expression for τ_{xx} is retrieved

$$\tau_{xx} = E\varepsilon_{xx}. \tag{A.69}$$

The rest of the stress components are equal to zero. For more details, one can follow [49].

Regarding double stresses, we adopt the following simplifications:

$$\mu_{i\alpha\beta} = 0, \quad \alpha, \beta = 2, 3, \; i = 1, 2, 3, \tag{A.70}$$

which eliminates $\partial_i\varepsilon_{\alpha\beta}$ in the constitutive relation (A.66) giving

$$\frac{\partial_x\varepsilon_{yy}}{\partial_x\varepsilon_{xx}} = \frac{\partial_x\varepsilon_{zz}}{\partial_x\varepsilon_{xx}} = -\frac{a_1+2a_2}{2(a_4+2a_2)}, \tag{A.71}$$

$$\frac{\partial_y\varepsilon_{yy}}{\partial_y\varepsilon_{xx}} = \frac{\partial_z\varepsilon_{zz}}{\partial_z\varepsilon_{xx}} = \frac{2a_4(a_1+2a_2)}{(a_1+2a_2)^2 - 4\bar{a}(a_2+a_4)}, \tag{A.72}$$

$$\frac{\partial_y\varepsilon_{zz}}{\partial_y\varepsilon_{xx}} = \frac{\partial_z\varepsilon_{yy}}{\partial_z\varepsilon_{xx}} = -\frac{(a_1+2a_2)^2 - 4\bar{a}a_2}{(a_1+2a_2)^2 - 4\bar{a}(a_2+a_4)}, \tag{A.73}$$

where $\bar{a} = a_1 + a_2 + a_3 + a_4 + a_5$. The active double stress components are redefined in the form

$$\mu_{xxx} = (2\bar{a} - \frac{(a_1+2a_2)^2}{a_4+2a_2})\partial_x\varepsilon_{xx}, \tag{A.74}$$

$$\mu_{yxx} = (2(a_2+a_4) + 2\frac{(a_1+2a_2)^2(a_4-a_2) + 4\bar{a}a_2^2}{(a_1+2a_2)^2 - 4\bar{a}(a_4+a_2)})\partial_y\varepsilon_{xx}. \tag{A.75}$$

It should be mentioned that within the simplified isotropic strain gradient elasticity [13, 47] which is derived by adopting $a_1 = a_3 = a_5 = 0$, $a_2 = \lambda g^2/2$ and $a_4 = \mu g^2$, the right hand sides of expressions (A.71), (A.72) and (A.73) degenerate into $-\lambda/2/(\mu+\lambda)$ which coincide with (A.68) for the classical case. On the other hand, the double stresses become $\mu_{xxx} = g^2E\partial_x\varepsilon_{xx}$ and $\mu_{yxx} = g^2E\partial_y\varepsilon_{xx}$ confirming that the higher-order assumptions are consistent with the classical ones.

It is also worth noting that relations (A.71)–(A.73) are derived by assuming that $\nabla\varepsilon_{xy} = \nabla\varepsilon_{xz} = \nabla\varepsilon_{yz} = 0$ in equations (A.70), which should be considered as one of the possible ways of deriving the higher-order beam model.

References

[1] G. A. Maugin, Generalized continuum mechanics: What do we mean by that?, in: G. A. Maugin, A. V. Metrikine (Eds.), Mechanics of Generalized Continua, One Hundred Years After the Cosserats, Springer, 2010, pp. 3–14.

[2] G. A. Maugin, A historical perspective of generalized continuum mechanics, in: H. Altenbach, G. A. Maugin, V. Erofeev (Eds.), Mechanics of Generalized Continua, Springer, 2011, pp. 3–14.

[3] D. D. Vescovo, I. Giorgio, Dynamic problems for metamaterials: Review of existing models and ideas for further research, International Journal of Engineering Science 80 (2014) 153–172.

[4] A. Carcaterra, F. dell'Isola, R. Esposito, M. Pulvirenti, Macroscopic description of microscopically strongly inhomogenous systems: A mathematical basis for the synthesis of higher gradients metamaterials, Archive for Rational Mechanics and Analysis 218 (2015) 1239–1262.

[5] E. Cosserat, F. Cosserat, Théorie des corps déformables, Paris, 1909.

[6] R. D. Mindlin, Micro-structure in linear elasticity, Archive for Rational Mechanics and Analysis 16 (1964) 51–78.

[7] A. E. Green, R. S. Rivlin, Multipolar continuum mechanics, Archive for Rational Mechanics and Analysis 17 (1964) 113–147.

[8] A. C. Eringen, Theory of micropolar elasticity, In: Leibowitz, H. (ed) Fracture 2 (1968) 621–629.

[9] P. Germain, The Method of Virtual Power in Continuum Mechanics. Part 2: Microstructure, SIAM Journal on Applied Mathematics 25 (1973) 556–575.

[10] R. A. Toupin, Elastic materials with couple-stresses, Archive for Rational Mechanics and Analysis 11 (1962) 385–413.

[11] R. D. Mindlin, Second gradient of strain and surface-tension in linear elasticity, International Journal of Solids and Structures 1 (1965) 417–438.

[12] R. D. Mindlin, N. N. Eshel, On first strain-gradient theories in linear elasticity, International Journal of Solids and Structures 4 (1968) 109–124.

[13] B. S. Altan, E. C. Aifantis, On some aspects in the special theory of gradient elasticity, Journal of the Mechanical Behavior of Materials 8 (1997) 231–282.

[14] F. Yang, A. Chong, D. Lam, P. Tong, Couple stress based strain gradient theory for elasticity, International Journal of Solids and Structures 39 (10) (2002) 2731–2743.

[15] D. C. C. Lam, F. Yang, A. C. M. Chong, J. Wang, P. Tong, Experiments and theory in strain gradient elasticity, Journal of the Mechanics and Physics of Solids 51 (2003) 1477–1508.

[16] H. Ma, X.-L. Gao, J. Reddy, A microstructure-dependent timoshenko beam model based on a modified couple stress theory, Journal of the Mechanics and Physics of Solids 56 (12) (2008) 3379–3391.

[17] B. Wang, J. Zhao, S. Zhou, A micro scale timoshenko beam model based on strain gradient elasticity theory, European Journal of Mechanics A/Solids 29 (2010) 591–599.

[18] K. A. Lazopoulos, A. K. Lazopoulos, Bending and buckling of thin strain gradient elastic beams, European Journal of Mechanics A/Solids 29 (2010) 837–843.

[19] S. Papargyri-Beskou, D. Beskos, Static analysis of gradient elastic bars, beams, plates and shells, The Open Mechanics Journal 4 (2010) 65–73.

[20] H. Askes, E. C. Aifantis, Gradient elasticity in statics and dynamics: An overview of formulations, length scale identification procedures, finite element implementations and new results, International Journal of Solids and Structures 48 (2011) 1962–1990.

[21] M. Asghari, M. H. Kahrobaiyan, M. Nikfar, M. T. Ahmadian, A size-dependent nonlinear timoshenko microbeam model based on the strain gradient theory, Acta Mechanica 223 (2012) 1233–1249.

[22] M. H. Kahrobaiyan, M. Rahaeifard, S. A. Tajalli, M. T. Ahmadian, A strain gradient functionally graded Euler–Bernoulli beam formulation, International Journal of Engineering Science 52 (2012) 65–76.

[23] M. Şimşek, J. N. Reddy, Bending and vibration of functionally graded microbeams using a new higher order beam theory and the modified couple stress theory, International Journal of Engineering Science 64 (2013) 37–53.

[24] M. Mohammad-Abadi, A. R. Daneshmehr, Size dependent buckling analysis of microbeams based on modified couple stress theory with high order theories and general boundary conditions, International Journal of Engineering Science 74 (2014) 1–14.

[25] J. Niiranen, V. Balobanov, J. Kiendl, S. Hosseini, Variational formulations, model comparisons and isogeometric analysis for Euler–Bernoulli micro- and nano-beam models of strain gradient elasticity, Mathematics and Mechanics of Solids, https://doi.org/10.1177/1081286517739669.

[26] V. Balobanov, J. Niiranen, Locking-free variational formulations and isogeometric analysis for the Timoshenko beam models of strain gradient and classical elasticity, in review for Computer Methods in Applied Mechanics and Engineering (2018).

[27] S. T. Yaghoubi, V. Balobanov, S. M. Mousavi, J. Niiranen, Variational formulations and isogeometric analysis for the dynamics of anisotropic gradient-elastic Euler–Bernoulli and shear-deformable beams, European Journal of Mechanics - A/Solids 69 (2018) 113–123.

[28] C. Liebold, W. H. Müller, Applications of strain gradient theories to the size effect in submicro-structures incl. experimental analysis of elastic material parameters, Bulletin of TICMI 19 (2015) 45–55.

[29] C. Liebold, W. H. Müller, Applications of higher-order continua to size effects in bending: theory and recent experimental results, in: H. Altenbach, S. Forest (Eds.), Generalized Continua as Models for Classical and Advanced Materials, Springer, 2016, Ch. 12, pp. 237–260.

[30] D. Polyzos, G. Huber, G. Mylonakis, T. Triantafyllidis, S. Papargyri-Beskos, D. E. Beskos, Torsional vibrations of a column of fine-grained material: A gradient elastic approach, Journal of the Mechanics and Physics of Solids 76 (2015) 338–358.

[31] N. C. Admal, J. Marian, G. Po, The atomistic representation of first strain-gradient elastic tensors, Journal of the Mechanics and Physics of Solids 99 (2017) 93–115.

[32] D. Adhikary, A. Dyskin, A Cosserat continuum model for layered materials, Computers and Geotechnics 20 (1997) 15–45.

[33] J.-J. Alibert, P. Seppecher, F. Dell'Isola, Truss modular beams with deformation energy depending on higher displacement gradients, Mathematics and Mechanics of Solids 8 (2003) 51–73.

[34] E. Pasternak, H.-B. Mühlhaus, Generalised homogenisation procedures for granular materials, Journal of Engineering Mathematics 52 (2005) 199–229.

[35] D. Adhikary, A. Dyskin, Modelling of progressive and instantaneous failures of foliated rock slopes, Rock Mechanics and Rock Engineering 40 (2007) 349–362.

[36] J. Romanoff, J. N. Reddy, Experimental validation of the modified couple stress timoshenko beam theory for web-core sandwich panels, Composite Structures 111 (2014) 130–137.

[37] J. Réthoré, C. Kaltenbrunner, T. B. T. Dang, P. Chaudet, M. Kuhn, Gradient-elasticity for honeycomb materials: Validation and identification from full-field measurements, International Journal of Solids and Structures 72 (2015) 108–117.

[38] M. Esin, A. Dyskin, E. Pasternak, Y. Xu, Mode I crack in particulate materials with rotational degrees of freedom, Engineering Fracture Mechanics 172 (2017) 181–195.

[39] S. Khakalo, J. Niiranen, Form II of Mindlin's second strain gradient theory of elasticity with a simplification: for materials and structures from nano- to macro-scales, revised for European Journal of Mechanics A/Solids (2018).

[40] J. Niiranen, S. Khakalo, V. Balobanov, A. H. Niemi, Variational formulation and isogeometric analysis for fourth-order boundary value problems of gradient-elastic bar and plane strain/stress problems, Computer Methods in Applied Mechanics and Engineering 308 (2016) 182–211.

[41] S. Khakalo, J. Niiranen, Isogeometric analysis of higher-order gradient elasticity by user elements of a commercial finite element software, Computer-Aided Design 82 (2017) 154–169.

[42] J. Niiranen, J. Kiendl, A. H. Niemi, A. Reali, Isogeometric analysis for sixth-order boundary value problems of gradient-elastic Kirchhoff plates, Computer Methods in Applied Mechanics and Engineering 316 (2017) 328–348.

[43] R. Makvandi, J. C. Reiher, A. Bertram, D. Juhre, Isogeometric analysis of first and second strain gradient elasticity, Computational Mechanics, (2017) doi:10.1007/s00466-017-1462-8.

[44] J. C. Reiher, I. Giorgio, A. Bertram, Finite-element analysis of polyhedra under point and line forces in second-strain gradient elasticity, Journal of Engineering Mechanics 143 (2017) 1–13.

[45] S. Thai, H.-T. Thai, T. P. Vo, V. I. Patel, Size-dependant behaviour of functionally graded microplates based on the modified strain gradient elasticity theory and isogeometric analysis, Computers and Structures 190 (2017) 219–241.

[46] A. E. H. Love, A treatise on the mathematical theory of elasticity, Fourth edition, Cambridge: University Press, 1927.

[47] M. Lazar, G. Po, The non-singular Green tensor of Mindlin's anisotropic gradient elasticity with separable weak non-locality, Physics Letters A 379 (24-25) (2015) 1538–1543.

[48] M. Lazar, G. A. Maugin, Nonsingular stress and strain fields of dislocations and disclinations in first strain gradient elasticity, International Journal of Engineering Science 43 (2005) 1157–1184.

[49] T. J. R. Hughes, The finite element method: linear static and dynamic finite element analysis, Dover Publications, Inc., 2000.

[50] R. G. Cowper, The shear coefficient in Timoshenko's beam theory, Journal of Applied Mechanics 33 (1966) 335–340.

[51] A. I. Borovkov, Effective physical and mechanical properties of fiber composites (in Russian), M.: Изд-во ВИНИТИ, 1985.

[52] V. A. Kuzkin, A. M. Krivtsov, E. A. Podolskaya, M. L. Kachanov, Lattice with vacancies: elastic fields and effective properties in frameworks of discrete and continuum models, Philosophical Magazine 96 (2016) 1538–1555.

[53] N. A. Fleck, V. S. Deshpande, M. F. Ashby, Micro-architectured materials: past, present and future, Proceedings of the Royal Society A 466 (2010) 2495–2516.

[54] R. Lakes, Foam structures with a negative Poisson's ratio, Science 235 (1987) 1038–1040.

[55] W. Yang, Z.-M. Li, W. Shi, B.-H. Xie, M.-B. Yang, Review on auxetic materials, Journal of Materials Science 39 (2004) 3269–3279.